

# **CORE ANALYSIS STUDY**

**Alberta Geological Survey**

**Alberta Energy Regulator**

**Various Wells**

**Canada**

## **FINAL REPORT**

### **Submitted to:**

**Arif Rabbani, PhD, PGeo**

**Alberta Geological Survey (AGS), Alberta Energy Regulator (AER).**

**August 15, 2025**

### **Performed by:**

**Core Laboratories**

**Petroleum Services Division**

**6316 Windfern**

**Houston Texas**

**202500182**

---

The analytical results, opinions, or interpretations contained in this report are based upon information and material supplied by the client for whose exclusive and confidential use this report has been made. The analytical results, opinions, or interpretations expressed represent the best judgement of Core Laboratories. Core Laboratories, however, makes no warranty or representation, express or implied, of any type, and expressly disclaims same as to the productivity, proper operations, or profitability of any oil, gas, coal, or other mineral, property, well, or sand in connection with which such report is used or relied upon for any reason whatsoever. This report shall not be reproduced, in whole or in part, without the written approval of Core Laboratories.

---

## Overview

We conducted multi-stage triaxial compressive strength tests on 24 rock specimen samples of various origins provided to us by the Alberta Geological Survey (AGS), Alberta Energy Regulator (AER). This work was completed under the Mineral Grant provided by the Government of Alberta, June 22, 2021. Specimens were of unknown origin to us but were predominantly hard (igneous/metamorphic) rocks, though a few hard sedimentary rocks were also provided. Of the 24 specimens tested, 11 were nominally 1.5" in diameter and 13 were 1" in diameter.

We were requested to perform multi-Stage Triaxial Compressive Strength (multi-stage) tests on all samples. More elaborate description of the methodology will be included below, but the general concept is to determine compressive strength at several different, increasing confining pressures, for the purposes of developing a Mohr-Coulomb failure envelope (i.e., determining coefficient of friction ( $m$ ) and cohesive strength ( $C_0$ )). All tests were performed with confining pressure stages of 1200, 2200, 4200, & 6200 psi. All tests were performed at elevated temperatures ranging from ~153 °F to ~389 °F.

For each specimen tested, during each confining pressure stage, we reported static Young's modulus & Poisson's ratio, compressive strength, and the Mohr-Coulomb failure envelope parameters.

Please see below for more detailed explanation of the specimen preparation, apparatus, and test procedure, as well as a general description of test results, with a more detailed description of selected test results.

In addition to the multi-stage testing performed by Core Laboratories, thermal expansion tests were conducted by a third-party vendor (Metarock Laboratories) on a total of 10 specimens, of these 10, two were twins of specimens on which multi-stage testing was also conducted (16 & 18). Temperatures were ramped from an initial value slightly above ambient to the in-situ temperature supplied by AGS. During the thermal expansion tests, ultrasonic velocity was measured twice, once at the initial, slightly above ambient temperature, and a second time at the final in-situ temperature.

## Sample Preparation

Specimens were provided to us already drilled from a host specimen. Thirteen samples were 1" in diameter, while 11 were 1.5" in diameter. Samples were largely tested at the diameter we received them, though one sample was sub-sampled from 1.5" diameter to 1" diameter due to the limited length of the specimen. Specimens were trimmed to avoid flaws to the extent feasible, while attempting to maintain as much length as possible (ideal L:D ratio ~2:1, minimum 1.4:1), though in one case we did test a shorter sample (24BA034, 1.33:1). The specimens were trimmed and the ends were ground square and parallel using a proprietary trimming/grinding machine in our rock shop. Length of the specimen was measured in 6 locations: once in the center, and once near each edge, rotated 90° and again measured in the center and at the edges. The allowable difference in length of these measurements was +/- 0.002" (i.e., +/- 0.1%). The diameter was measured in 9 locations, once at the top, middle, and bottom of the sample, rotate by 60° & repeat measurements, and a final 60° rotation and repetition of the measurements. For diameter there was no real threshold given that the plugs were drilled as cylinders, though no plug had variation of more than +/- ~0.004" and most were ≤ +/- ~0.002.

Following preparation of the ends, the specimens were jacketed in a fluorinated ethylene propylene (FEP) heat shrink tube to isolate it from the confining medium in the pressure cell. The jacketed specimen was then affixed to steel loading platens, with the pore fluid ports vented to the atmosphere. Two Axial Deformation sensors, linear variable differential transformer (LVDTs) were affixed to the loading platens to

measure axial shortening during the testing, and one circumferential deformation sensor was utilized (Figure 1).

Specimens used for thermal expansivity measurements were prepped in a comparable manner prior to being provided to Metarock Laboratories for testing.

## **Apparatus**

### **Used for Multi-Stage Testing**

Tests were conducted in an RTX-4000 load frame manufactured by the GCTS corporation (Figure 2). This apparatus is a conventional triaxial load frame, in which a hydrostatic confining pressure is applied to the specimen (i.e., Confining Pressure ( $P_c$ ) =  $s_2 = s_3$ ). Axial load was then applied using a loading piston along axis with the testing specimen, driven by a servo-controlled hydraulic ram. The maximum capabilities of the load frame are 30,000 psi for both confining pressure and pore pressure (though pore pressure was not utilized for this testing program), and 1,000,000 lbf from the axial loading column.

Tests were conducted at elevated temperatures ranging from ~153 °F (67 °C) to ~389 °F (198.3 °C). Heating was accomplished via two external heating bands wrapped around the outside of the pressure cell. In order to expedite timing of testing program, specimens were not allowed to reach complete thermal equilibrium prior to testing but rather were allowed to heat to a point where confining pressure feedback no longer indicated overall expansion of the confining fluid, but rather only cyclic heating and cooling around the set point. In other words, the temperature had reached the set point, but was not stable, rather it cycled around the set point in a roughly sinusoidal manner, with the temperature fluctuating generally less than +/- 7 °F around the set point temperature. This method was used because it very likely would have at least doubled the time required for each test to achieve anything approaching true equilibrium, which would have resulted in the project overrunning the required end date. Specimens were heated for 6-10 hours to achieve the rough, sinusoidal quasi-equilibrium, with the heating time largely being dependent on the absolute temperature used.

The specimens used for testing were, as mentioned previously, jacketed in FEP shrink tube to isolate them from the confining medium, which in all cases was hydraulic fluid. The jacketed specimens were affixed to steel end caps (platens), the pore fluid system was vented to the atmosphere for all tests. Axial deformation was measured via two Linear Variable Differential Transformers (LVDTs) aligned along axis with the plug, the output of which was averaged to determine axial strain. Given that the axial deformation sensors are mounted onto the steel end caps, some portion of the axial deformation measured during testing was from deformation of the platens themselves, the stiffness of the loading platens is calibrated, and this portion of the total deformation was removed from the measurement of the specimen deformation. Radial strain was measured via the use of a so-called "chain gauge" that wraps around the circumference of the specimen, with a third LVDT that measures the opening/closing of the gap between the ends of the chain. See Figure 1 for a schematic representation of the sample assembly.

### **Used for Thermal Expansion Testing**

Thermal expansion testing is performed by heating a rock specimen from an initial temperature nominally above ambient to a pre-selected temperature of interest and measuring the axial expansion of the specimen as a result. The apparatus used for this testing is a small hydrostatic pressure cell into which the sample assembly shown in Figure 3 is fitted. As with the multi-stage testing the specimen was fitted between two steel loading platens. Two axially oriented LVDTs were mounted onto the platens, though in this case an elastic calibration is not necessary because the specimen is kept at constant confining

pressure through the duration of the test, resulting in no changes in the elastic deformation of the platens. Radial strain was measured using a cantilever bridge style strain gauge, allowing for the measurement of radial strain in two orthogonal directions. The specimen was heated using a proprietary sleeve type heating element that fits closely around the specimen. Ultrasonic velocity was measured via piezoelectric crystals embedded into the steel loading platens, that generate the P-waves and S-waves at one end of the specimen, which then travel through the specimen, and are received by crystals in the opposite platen.

## Procedure

### Multi-Stage Triaxial Compressive Strength Testing

Creating a Mohr-Coulomb failure envelope in the conventional manner involves measuring the compressive strength of multiple rock specimens (of the same type) at different confining pressures. Our internal procedure typically involves conducting one unconfined compressive strength (UCS) test, and three triaxial compressive strength (Triax) tests at different confining pressures. Typically, we see that compressive strength increases as a function of increasing confining pressure (Figure 4). We then generate a plot of compressive strength v. confining pressure, and plot Mohr's circles of the stress conditions at failure (Figure 5). A best fit tangent line to those Mohr's circles provides the so-called "Mohr-Coulomb failure envelope," the slope of which is the coefficient of friction of the intact rock, and the intercept is its cohesive strength (i.e., the shear strength at zero normal stress).

The general purpose of "multi-stage" triaxial compressive strength tests is to achieve something similar to the typical testing procedure for creating a Mohr-Coulomb failure envelope by performing, but by performing only a single test on one plug. The conventional means of performing a multi-stage test involves applying a confining pressure to a specimen, loading the specimen axially, and (largely by observing the shape of the Differential Stress v. Axial Strain curve) determining that the specimen is closely approaching shear failure so that loading can be halted and reversed. After axial load is removed, the hydrostatic confining pressure is increased, and the process is repeated, loading the specimen axially until failure appears imminent, then halting & reversing the axial loading. In our laboratory this process is typically repeated for a 3<sup>rd</sup> and 4<sup>th</sup> Stage, however during the 4<sup>th</sup> Stage the specimen is loaded completely to failure. In this way the results of the experiment provide a value close to the failure strength of the specimen at several increasing confining pressures (Figure 6). The results of the test can then be used, just as with the results of several tests on several plugs at different confining pressures, to create a Mohr-Coulomb failure envelope (Figure 7). The main advantage of the multi-stage test is the capability of developing a failure envelope in scenarios where sample availability is limited, drawbacks are that while they generally produce values for coefficient of friction and cohesive strength that match up well with envelopes developed from tests on multiple specimens, the latter stages of the test run the risk of being influenced by the damage imparted upon the rock by repeatedly bringing it close to failure (in particular, the elastic parameters measured during the latter stages of a conventional multi-stage test can be negatively influenced). Additionally, by bringing the rock so close to failure over and over, there is a risk of the specimen failing accidentally before the entire test procedure can be completed.

To mitigate some of the concerns of conventional multi-stage testing, we have developed a procedure based on utilizing volumetric strain to identify a systematic point to unload the specimen earlier during axial loading, alleviating some of the concern of significantly damaging the sample by repeated loading and also limiting the likelihood of premature failure. In most ways the test is self-similar to the above description for the conventional multi-stage procedure with the exception that rather than continuing axial loading until failure appears imminent we load the specimen until volumetric strain ( $\epsilon_v$ ) indicates that

deformation of the plug has transitioned from volumetric compression to dilation (a point that often closely coincides with yield strength, after which some portion of the loading of the specimen is plastic rather than elastic, i.e. some portion of the deformation of the specimen is permanent). We do this during each of Stages 1-3, unloading the specimen when  $e_v$  transitions from compression to dilation. During Stage 4 we note the point of  $e_v$  transition, but continue loading to failure, just as in the conventional multi-stage test (Figure 8). We then use the trend of “Axial Stress at the point of  $e_v$  transition” versus  $P_c$ , and scale that line up to the failure strength observed during Stage 4 and then use these estimated failure strengths to create a Mohr-Coulomb failure envelope (Figure 9). We have found, based on internal testing, that this produces a trend that is similar to both conventional multi-stage testing and also to multiple single-stage tests at different confining pressures. The method is not fool proof in that not all rocks exhibit the volumetric transition prior to failure but rather continue to display volumetric compression throughout loading, this is particularly common in high porosity or poorly lithified rocks. In such cases we typically recommend against performing multi-stage tests altogether, or default back to the conventional multi-stage method if failure appears imminent prior to the volumetric transition. The tests performed for this study were all of the volumetric strain multi-stage type.

After the testing specimen was prepped, jacketed, and mounted onto the loading platens, as described above in the “sample preparation” section, the pressure cell wall was lowered over the sample assembly and then filled with hydraulic fluid. Once full, the heating bands were turned on and the pressure cell & sample were raised to the target temperature for the test. During most of the heating phase the cell was left vented to the atmosphere so that pressure did not build up as the heating fluid expanded. Towards the end of heating the pressure was increased to a constant 200 psi so that we could determine via nominal stabilization of the fluid volume that the system had fully reached the target temperature and was at that point only cycling sinusoidally around the target. At this point, the hydrostatic confining pressure was increased to the initial testing value, 1200 psi for all tests. The duration of the initial heating stage ranged from ~6 to ~10 hours, the duration being nominally correlated to the target temperature.

Once the initial confining pressure was applied, the specimen was allowed to equilibrate to this initial stress state. Given that this project was largely conducted on igneous, metamorphic, and hard sandstone specimens, only a few minutes was typically necessary to reach equilibrium, which we judge as a quasi-flatlining of the radial strain output as a function of time. Upon reaching equilibrium, axial loading of the specimen was performed at a constant strain rate (nominally  $5 \times 10^{-6}/s$ ). During the test differential stress, confining pressure, temperature, axial strain, radial strain, and volumetric strain were constantly monitored. As described in more detail above, axial loading continued until volumetric strain transitioned from bulk compression to bulk dilation. Once we observed the transition from volumetric compression to dilation (we generally allowed loading to continue just beyond the transition to be sure) axial load was removed. After the removal of axial load, the confining pressure was increased to the Stage 2 value (2200 psi in all tests), and axial loading was recommenced at a nominal strain rate of  $5 \times 10^{-6}/s$  until the  $e_v$  transition was observed, and axial load was removed. Stage 3 progressed similarly at  $P_c = 4200$  psi, followed by Stage 4 at  $P_c = 6200$  psi, though during Stage 4 the point of  $e_v$  transition was observed, but axial loading was continued until the specimen failed.

After failure, axial load was removed, the confining pressure brought down to zero, and the heating bands were shut off. The specimen and load frame were allowed to cool overnight. The next morning the pressure cell was drained and opened, and the specimen was removed from the loading platens, and returned to storage.

## Thermal Expansivity & Ultrasonic Velocity Testing

After the jacketed and instrumented specimen was loaded into the pressure cell, the cell was closed and filled with heat transfer fluid. Confining pressure was raised to an initial value of 100 psi, followed by heating to an initial temperature of 30 °C. The specimen was given time to equilibrate to these conditions, after which the confining pressure was raised to the in-situ value at a rate of 1 psi/sec. At this point, with an in-situ confining pressure and an initial temperature of 30 °C, the specimen was allowed to equilibrate for up to several hours. At the end of the equilibration phase the initial measurement of P-wave and S-wave velocity were made. Following the ultrasonic velocity measurement, the temperature was raised to the target value at a rate 18 °C/hr. Once the specimen reached the target temperature the elevated temperature ultrasonic velocity measurements were performed, and the specimen was allowed to equilibrate there for ~1-4 hours before temperature was reduced back to 30 °C at the same rate of 18 °C/hr. For the duration of the test confining pressure was held constant, and the axial and radial deformation were monitored throughout. The thermal expansion coefficient was determined, in all cases, during the ramp up to the in-situ temperature (as opposed to the ramp back down to 30 °C) via the slope of the axial strain v. temperature curve, though the slope on the ramp back down was nominally very similar.

## Overview of Results and Discussion of Selected Results

### Multi-Stage Results - General Overview

The complete results of multi-stage triaxial compressive strength testing on 24 specimens are shown in Tables 1 & 2. Plots containing summaries of all the data are far too crowded to show in a review document such as this, please see the provided final data report which includes plots of all data types that allow for filtering to see only selected specimen results. The estimated unconfined compressive strength (UCS) for the specimens, which is based on the trend of compressive strength v. confining pressure observed during the multi-stage tests, ranged from ~3200 psi (specimen BCS 1 (25BCS001)) to nearly 64,000 psi (Specimen 24BA073), with the bulk of the specimens exhibiting an estimated UCS between ~13,500 psi ~33,500 psi. Specimen 24BA073 was by far the strongest of the samples we evaluated, with compressive strength ranging from 73,934 psi at  $P_c=1200$  psi to 116,960 psi at  $P_c=6200$  psi, this is one of the strongest rocks we have ever tested in our laboratory. Specimens 24BA018 & BCS 1 were the weakest specimens tested with strength ranging from ~11,400 psi at  $P_c=1200$  psi to ~44,000 psi at  $P_c=6200$  psi. Specimen 24BA0434 was also comparatively weak, perhaps weaker than either of the aforementioned specimens, but the test on this specimen failed during Stage 1, and therefore no estimate of UCS was feasible. Further, the test conducted on specimen BCS 1 was difficult to interpret due to a leak that developed in the jacket between Stages 3 & 4, that negatively influenced the result of Stage 4, regardless of that however, BCS 1 was certainly among the weakest rocks tested. While these were the weakest samples tested as part of this study, they are by no means objectively “weak,” we test many rocks as part of our more typical projects (oil & gas related sands, carbonates, and shales) that are far weaker than these specimens.

Static Young's modulus correlates very well with compressive strength, and we see that with these specimens, observing generally quite high Young's moduli values to go along with the high compressive strengths (Figure 10). Specimen 24BA073, in addition to being the strongest sample tested, was also the stiffest (though not by as wide a margin), exhibiting a static Young's modulus ranging from ~13.8 Mpsi at  $P_c=1200$  psi to ~12.9 Mpsi at  $P_c=6200$  psi. We typically observe that Young's modulus increases with increasing confining pressure, that we see the opposite in this case suggests that even though we utilized a multi-stage method specifically meant to avoid doing so, the specimen may have been slightly damaged

by repeated loading. Specimen BCS 1, as it was the weakest specimen tested, was also the most compliant, exhibiting a static Young's modulus ranging from ~3.7 Mpsi during stage 1 to ~6.7 during stage 3 (recall that the specimen developed a leak between Stage 3 & Stage 4, resulting in compromised results for Stage 4). Specimen 24BA034 (which failed during Stage 1) was also relatively compliant, with a static Young's modulus of ~3 Mpsi.

The static Poisson's ratio of the specimens was relatively tightly grouped, with the majority of test results indicating a Poisson's Ratio between 0.2 & 0.3, with a handful of results slightly lower (minimum of 0.13) and higher (maximum of 0.35). In general we did not observe large changes in static Poisson's ratio from one stage to the next, though most tests did exhibit a modest increase from Stage 1 to Stage 2, again suggesting the possibility that the specimens may have been slightly damaged during loading, despite our attempts to avoid this.

### **Thermal Expansivity & Ultrasonic Velocity Results – General Overview**

Thermal expansivity values ranged from  $-4.58 \times 10^{-6}$  in/in/°C to  $-7.87 \times 10^{-6}$  in/in/°C (Table 3). No sample particularly stuck out as being particularly high or low compared to the others.

Ultrasonic velocity was measured both at the beginning of the heating and at the end (i.e. at 30 °C and at the final in-situ temperature), all specimens showed a decrease in both P-wave velocity and S-wave velocity at the higher temperatures, though the P-wave velocity for specimen 5 (Depth: 1833.33 m) only showed a negligible reduction of 7 ft/sec (Table 4). The velocities themselves were generally quite high, with P-wave velocity ranging from 15,358 ft/s to 21,955 ft/s at in-situ temperature, and S-wave ranging from 9758 ft/s to 13,146 ft/s. The few samples that were towards the lower end of this range are comparable to the specimens we typically examine in our laboratory, while those at the higher end are among the fastest rocks we have tested. Dynamic Young's moduli ranged from 7.35 Mpsi to 14.89 Mpsi, while dynamic Poisson's Ratio ranged from -0.03 to 0.28, it must be presumed that the -0.03 value represents some sort of complication in the measurement.

There did not appear to be significant correlation between ultrasonic velocity and thermal expansivity.

### **Multi-Stage Testing - Selected Specimen Specific Results**

24BA025 (Depth: 1111.00 m) – A Type Example of the Volumetric Multi-Stage Test

The multi-stage test conducted on specimen 24BA025 was a good example of an ideal result for this style of test. During each of the four stages of the test, there was a clear transition from volumetric compression to volumetric dilation (Figure 11) that gave us indication to halt axial loading and unload the specimen, before increasing the confining pressure to the next stage value. The compressive strength of the specimen ranges from nearly 38,000 psi at  $P_c=1200$  psi to almost 61,000 psi at  $P_c=6200$  psi, with an estimated UCS of ~32,000 psi. While this strength is middle-of-the-pack for the specimens tested as part of this project, it is quite strong compared to most of the specimens tested in our laboratory.

Elastic parameters differ slightly from the first stage to the last when measured in our default location (data range from 45-55% of the maximum differential stress), though less so when measured slightly earlier in the loading curve (from ~15-40% maximum differential stress), which quite often yields more consistent measurements of elastic properties during multi-stage tests. Static Young's modulus decreased from each stage to the next (when measured from 45-55% of the maximum differential stress) from ~10.3 Mpsi during Stage 1 to ~9.7 Mpsi during stage 4, however when measured earlier during loading (~15-40% of maximum differential stress), the Young's modulus remains essentially constant from stage to stage (see test tab for specimen 24BA025 in the summary data file). Static Poisson's Ratio increased slightly from ~0.21 to ~0.28 from the first stage to the last (when measured over the data range from 45-

55% of the maximum differential stress), though again the variation was less (~0.19-0.23) when measured earlier during loading.

Mohr-Coulomb analysis of the results of the test on specimen 24BA025 indicates a coefficient of friction of ~0.85 with a cohesive strength of ~7400 psi (Figure 12). Both values are middle-of-the-pack for the specimens tested as part of this project. The amount of scaling from the axial stress at the transition from volumetric compression to dilation up to the failure strength observed during Stage 4 was relatively modest compared to many of the specimens tested here.

#### 24BA073 (Depth: 2101.17 m) – The Strongest Specimen Tested

Specimen 24BA073 was, by a wide margin, the strongest rock tested as part of this project, and also the stiffest. Based on the shape of the differential stress v. axial/radial Strain curves (Figure 13) there was, outside of the specimen's exceptional strength and stiffness, nothing unusual about the result. Figure 14 shows the Mohr-Coulomb envelope data, and likewise there is nothing particularly unusual about the result outside of the fact that it is an extremely strong rock. Sample 24BA073 displays the highest coefficient of friction for the intact sample (1.30) of the specimens tested, though there are many other samples that exhibited a friction coefficient in excess of 1.1.

Specimens 18 (25BA031, depth: 2101.17 m) and 16 (25BA029a, depth: 3027.20 m) – Tested for both compressive strength and thermal expansivity & ultrasonic velocity

The plugs provided to us for testing were, in two cases, long enough that they could be trimmed approximately in half, producing two specimens that were long enough for both multi-stage compressive strength testing and for the thermal expansivity/ultrasonic velocity measurements performed by Metarock Laboratories.

Specimen 18 was by a wide margin the stronger of the two, with strength ranging from ~27,400 psi at  $P_c=1200$  psi to ~60,200 psi at  $P_c=6200$  psi, with an estimated UCS of ~19,600 psi. Static Young's modulus increased from ~8.9 Mpsi during Stage 1 to ~10.9 Mpsi during Stage 3 (with a small reduction to 10.8 Mpsi during Stage 4), the increase being a strong indication the sample was not significantly damaged by repeated loading. Static Poisson's ratio was relatively stable during the test ranging from ~0.18 to ~0.26. Specimen 18b displayed a thermal expansivity of  $-7.31 \times 10^{-6}$  in/in/°C over a temperature range from 30-116 °C. P-wave velocity decreased slightly, from 20,819 ft/sec to 20,413 ft/sec over the temperature range, S-wave velocity also decreased slightly from 12,402 ft/sec to 12,114 ft/sec. The dynamic Young's modulus for the specimen ranged from 13.3-13.9 Mpsi, a factor of ~30-50% higher than the static moduli, and the dynamic Poisson's ratio was 0.22-0.23, which compares well with the range of static values we measured.

The strength of specimen 16 ranged from ~19,500 psi at  $P_c=1200$  psi to ~36,300 psi at  $P_c=6200$  psi, with an estimated UCS of ~15,500 psi. Static Young's modulus increased from ~4.5 Mpsi during Stage 1 to ~5.7 Mpsi during Stage 4, the increase being a strong indication the sample was not significantly damaged by repeated loading. Static Poisson's ratio was somewhat stable during the test ranging from ~0.19 to ~0.27. Specimen 16b displayed a thermal expansivity of  $-7.15 \times 10^{-6}$  in/in/°C over a temperature range from 30-167 °C. P-wave velocity decreased slightly, from 16,046 ft/sec to 15,358 ft/sec over the temperature range, as did S-wave velocity, decreasing from 10,378 ft/sec to 9758 ft/sec. The dynamic Young's modulus for the specimen ranged from 7.3-8.1 Mpsi, a factor of ~40-60% higher than the static moduli, and the dynamic Poisson's ratio of 0.15-0.16 was slightly lower than the static values measured.



Specimen 24BA034 (Depth: 1762.51 m) – Failed during stage 1

Specimen 24BA034 was the very first specimen we tested as part of this project, at which point we were not sure how these hard rocks would respond to multi-stage testing. We typically will push a bit beyond the  $e_v$  transition to be certain that we have captured the turnaround, however it seems that some of these hard, and quite brittle rocks, are very susceptible to failure with any significant amount of volumetric dilation. In the case of the test performed on this sample, we pushed the axial loading too far past the volumetric transition and it failed. This is somewhat unfortunate in the sense that it appears that this is likely to be the weakest of the specimens tested, with a compressive strength of only ~7800 psi at  $P_C=1200$  psi, and therefore having a fuller understanding of the behavior of this relatively weak specimen would have been valuable to the study.

#### **Other unusual results worth highlighting**

Specimen 24BA067 appears to have developed a leak at some point during loading of Stage 4. Loading seemed to be progressing similarly to what was seen during Stages 1-3 when there was an abrupt failure like feature observed in the loading curve, and ultimately the specimen failed at a lower differential stress than the maximum achieved during Stage 3. As a result, when developing the Mohr-Coulomb failure envelope, we were only able to use the results from Stages 1-3, and were forced to presume that the maximum stress achieved during Stage 3 was close to the compressive strength, which may well have been the case given the very slight failure feature that was observed at the end of Stage 3 loading.

Specimen 24BA018 exhibits a significantly lower static Young's modulus during stage 4 (7.4 Mpsi) than during Stage 3 (11.0 Mpsi). It also shows a significantly higher static Poisson's Ratio during Stage 4 (0.34) than Stage 3 (0.24). It is possible that the specimen was significantly damaged during Stage 3 loading, leading to the decreased Young's modulus and increased Poisson's ratio, which may be born out by observing the shape of the differential stress v. axial strain plot for stage 3, which displays significant rollover, which is very likely due to the creation and growth of cracks in the specimen leading to plastic deformation.

Three of the four Hunt well specimens (#13 (25BA\_HW\_013), #18 (25BA\_HW\_018), & #27 (25BA\_HW\_027)) displayed an extraordinary amount of continued strengthening beyond the  $e_v$  transition during Stage 4 loading. All of the Hunt well specimens are relatively strong (including #21 ((25BA\_HW\_021) which did not exhibit the significant post- $e_v$  transition strengthening), only exceeded by the aforementioned 24BA073 specimen, and equaled by 24BA004. They all exhibit comparatively high values for static Young's modulus, which makes sense considering their strength, and extremely self-similar values for static Poisson's Ratio with all for specimens ranging from ~0.28 during Stage 1 to ~0.33 during Stage 4, which is towards the high end of Poisson's' Ratio values measured for this project. In general, the specimens are very self-similar, and unique (with the exception of Hunt Well #21) in the degree of continued strengthening we observed beyond the transition from volumetric compression to dilation.

## Figures

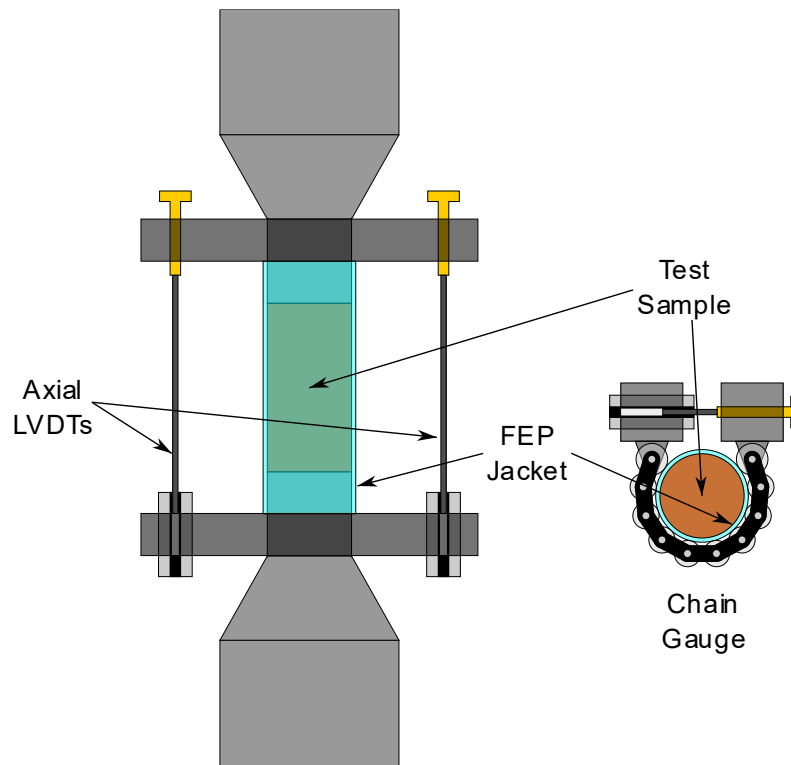


Figure 1: Left - Schematic representation of the jacketed sample affixed to the axial loading platens. Axial deformation is the average output of two axially oriented LVDTs. Right – Schematic representation of the “chain gauge” that wraps around the specimen, an LVDT in the blocks at the end of the chain gauge measures the changes in cord length of the opening of the chain, which is translated into radial strain.

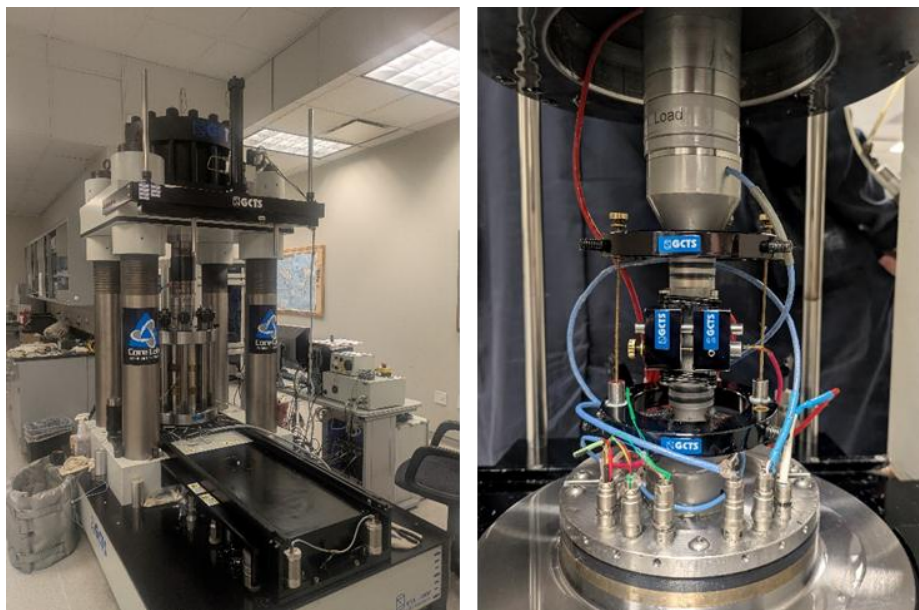


Figure 2: Left - RTX-4000 conventional triaxial load frame, used for conducting multi-stage triaxial compressive strength tests for this project. Right – Close view of sample assembly in load frame.

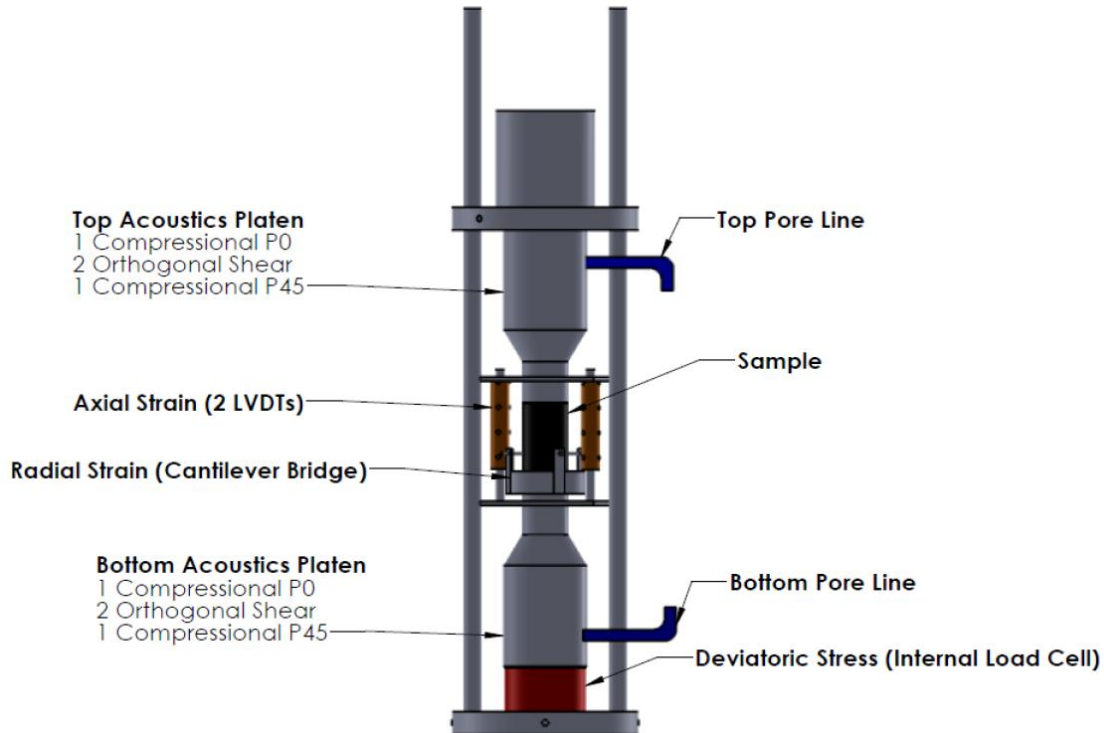


Figure 3: Schematic of apparatus used by Metarock Laboratories to perform thermal expansion measurements, and also ultrasonic velocity in conjunction with the TE testing. This sample assembly is fitted inside a small hydrostatic pressure cell and is heated with a proprietary, sleeve style heating unit that is fitted around the specimen.

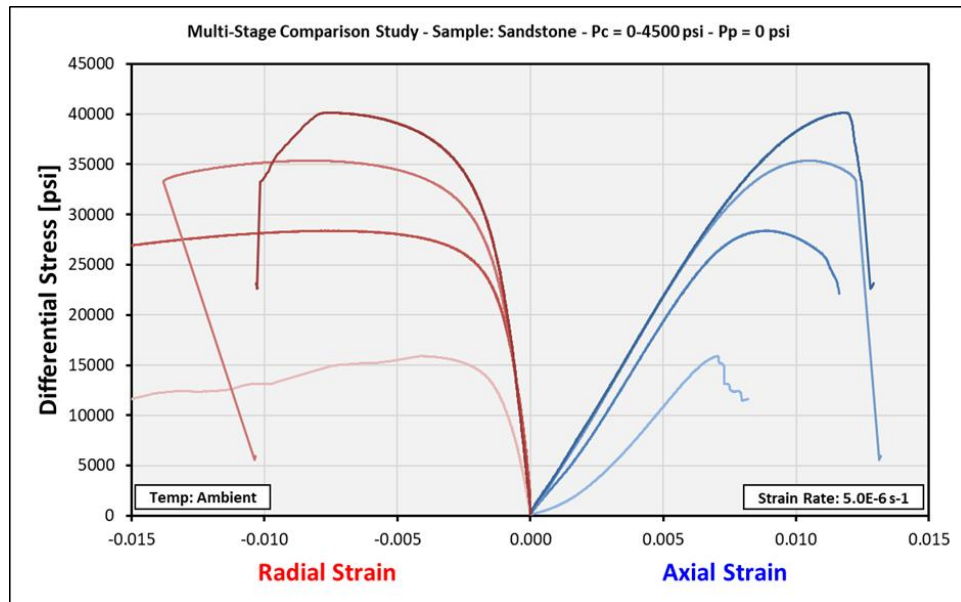


Figure 4: Results of four separate triaxial compressive strength tests conducted at different confining pressures for the purposes of creating a Mohr-Coulomb failure envelope. In this example tests were performed at confining pressures of 0 (UCS), 1500, 3000, and 4500 psi.

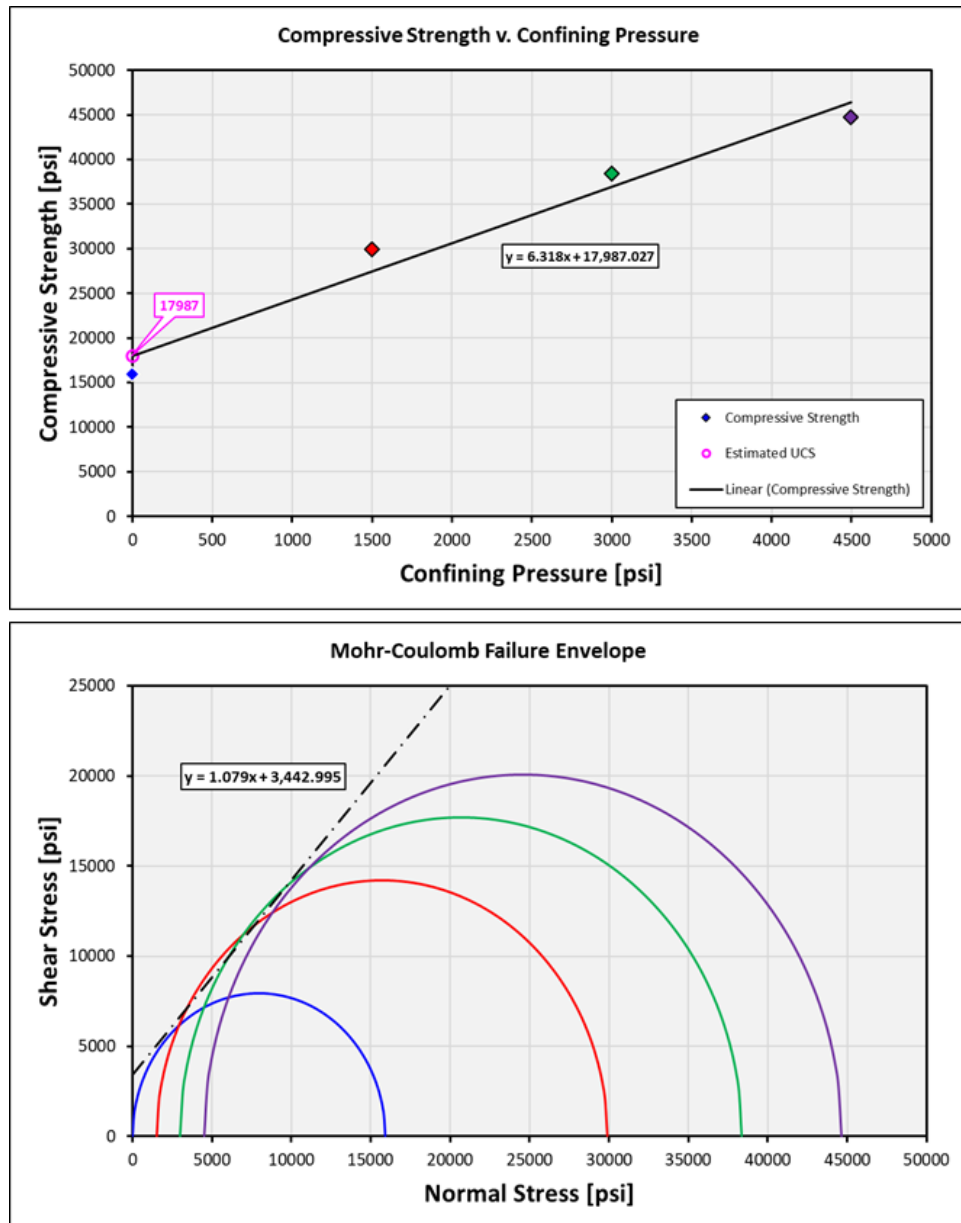


Figure 5: Top - compressive strength v. confining pressure for typical testing used to determine Mohr-Coulomb failure envelope, multiple triaxial compressive strength tests performed at different confining pressures. Bottom - Mohr-Coulomb failure envelope generated using the results shown in the Top plot, indicating a coefficient of friction of ~1.08 and a cohesive strength of ~3443 psi.

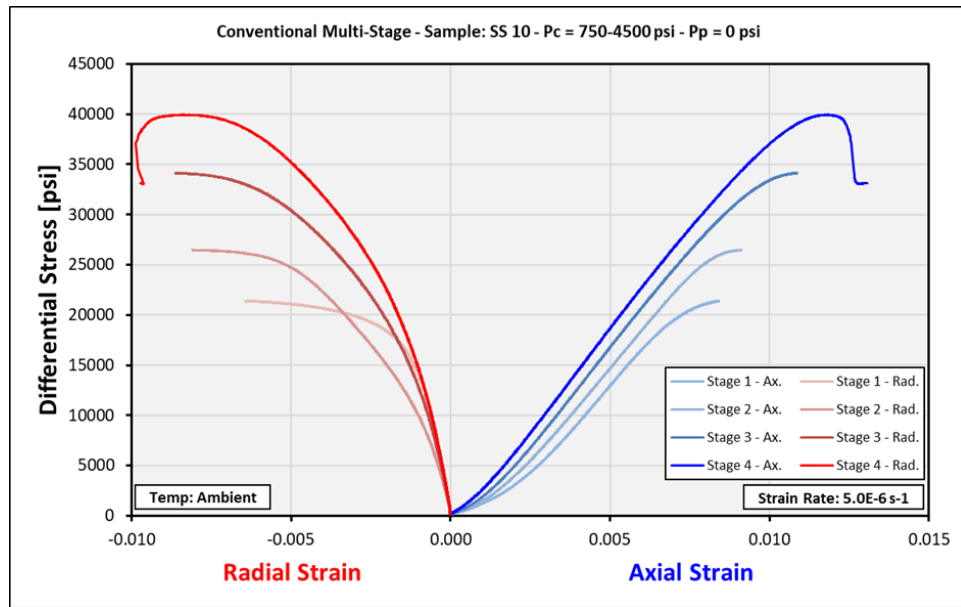


Figure 6: Results of a conventional multi-stage triaxial compressive strength test conducted at four increasing confining pressure stages (750, 1500, 3000, and 4500 psi). Note that during each state the specimen was loaded axially until failure appeared to be imminent based on the shape of the differential stress v. axial strain curve. By loading the specimen so close to failure, it is certainly damaged, potentially influencing the observed strength displayed during each stage after the first. The volumetric strain version of the multi-stage test is our attempt to alleviate the potential influence of damage to the specimen.

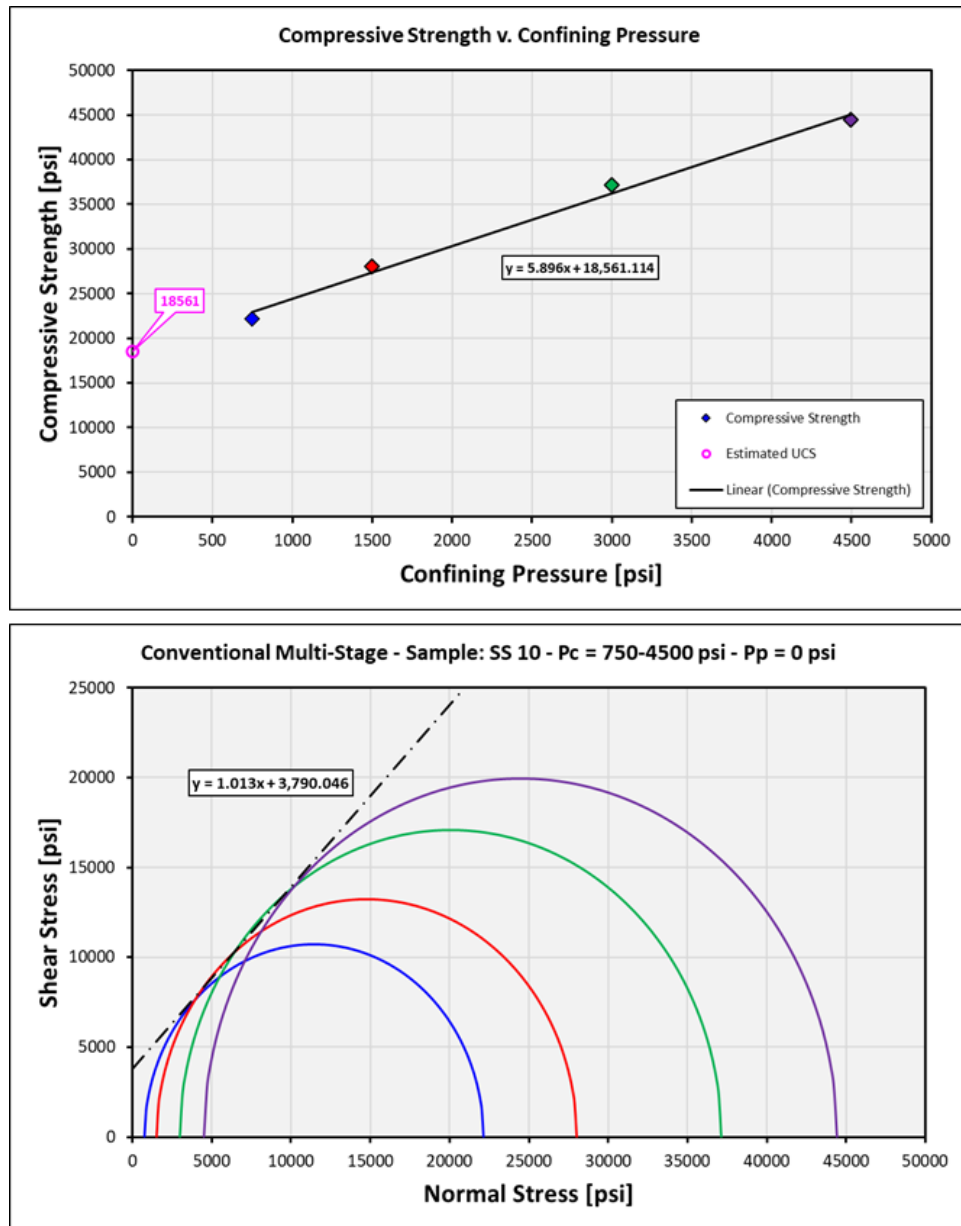


Figure 7: Top - Compressive strength v. confining pressure from the results of a conventional multi-stage test, multiple values closely approximating the compressive strength of a single specimen at four increasing confining pressures, used to determine Mohr-Coulomb failure envelope. Bottom - Mohr-Coulomb failure envelope generated using the results shown in the top plot, indicating a coefficient of friction of ~1.01 and a cohesive strength of ~3790 psi.

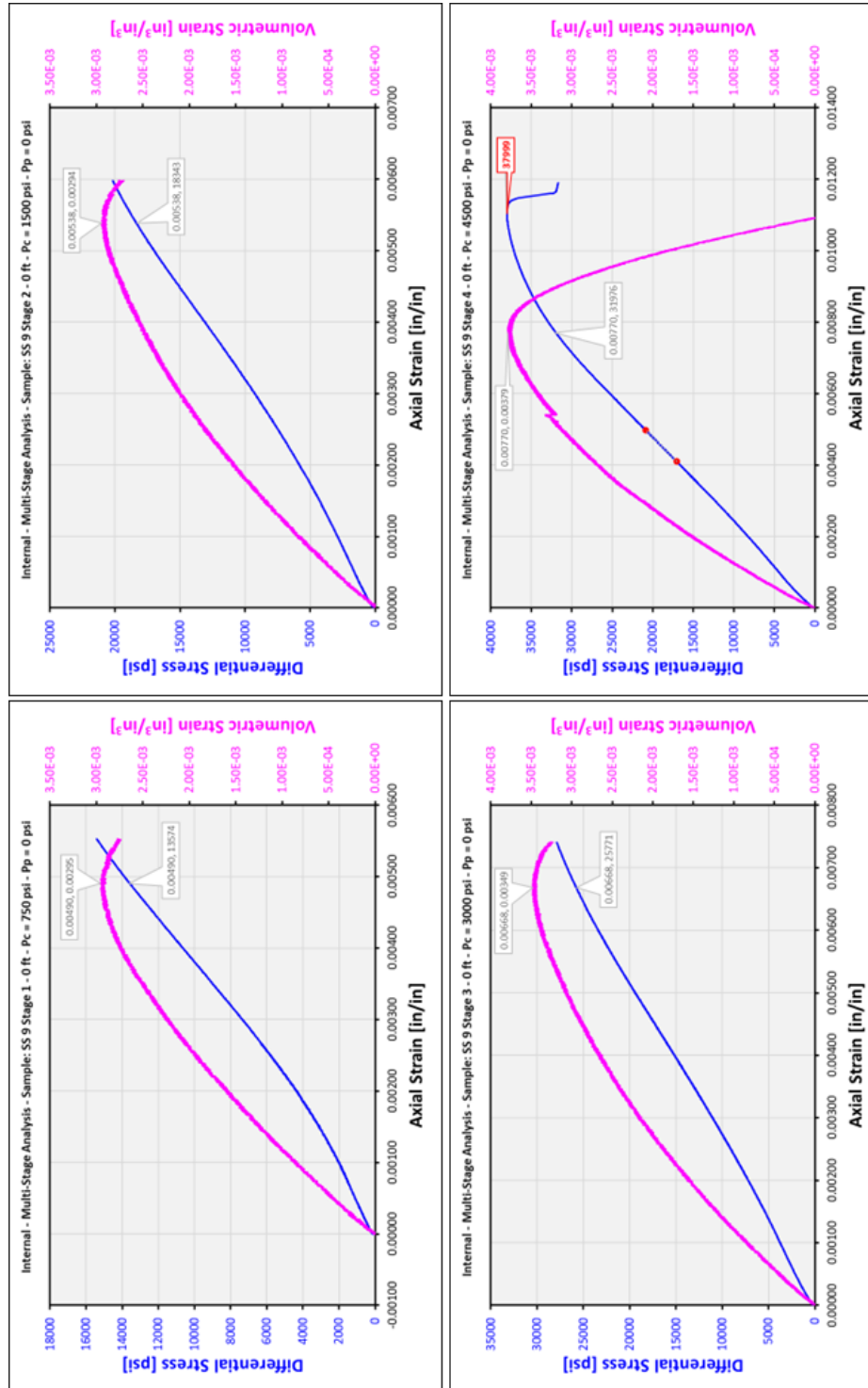


Figure 8: Results of the four separate stages of a multi-stage test performed using the volumetric Strain procedure. During each confining pressure stage (750, 1500, 3000, and 4500 psi) the specimen is loaded axially until we observed the transition from volumetric compression to dilation, at which point axial load is removed and a higher confining pressure is applied. As with the conventional multi-stage method, axial loading during Stage 4 is continued until shear failure is observed.

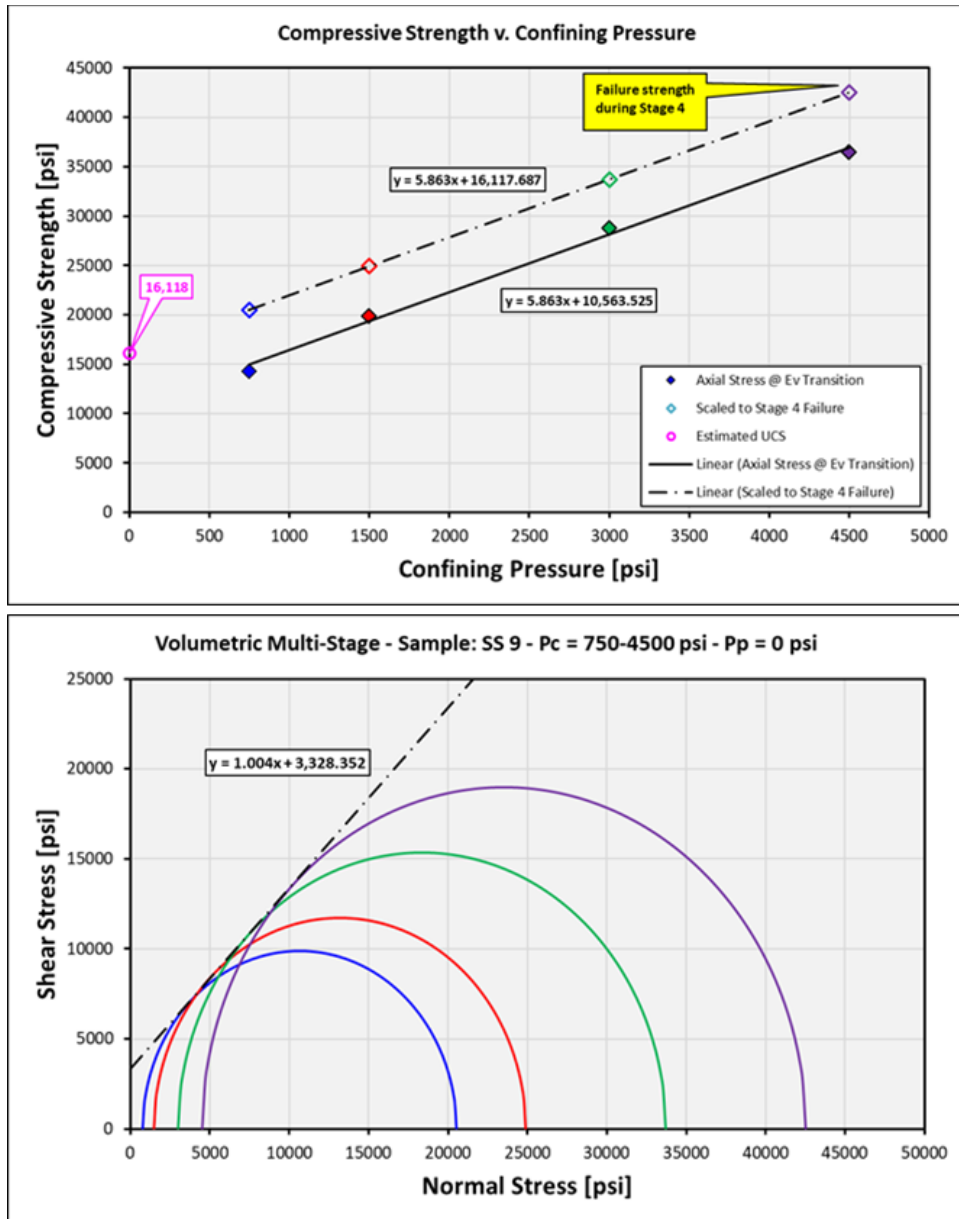


Figure 9: Top - compressive strength v. confining pressure from the results of a volumetric strain multi-stage test. The Axial stress at the point of transition from volumetric compression to dilation is plotted versus confining pressure (solid data point & solid line), this line is then scaled up to the compressive strength observed during Stage 4 to approximate the compressive strength during each stage of the test, which is then used to create the Mohr-Coulomb failure envelope. Bottom - Mohr-Coulomb failure envelope generated using the results shown in the top plot, indicating a coefficient of friction of ~1.004 and a cohesive strength of ~3330 psi.



Sample Number [-]	Depth [in]	Sample Length [in]	Sample Diameter [in]	L:D Ratio [-]	As-Tested Bulk Density (g/cm <sup>3</sup> )	Stage [-]	Set Point Temperature [°F]	Confining Pressure [psi]	Pore Pressure [psi]	Scaled Compressive Strength [psi]	Compressive Strength [psi]	Static Young's Modulus [MPa]	Static Young's Modulus [GPa]	Static Poisson's Ratio <sup>(1)</sup> [-]	Estimated UCS [psi]	Coefficient of Friction [-]	Cohesive Strength [psi]
24BA025	1111.00	2.8284	1.4785	1.91	2.68	1	153	1200	0	37617		10.30	71.0	0.211	32031	0.85	7423
	1111.00					2	153	2200	0	42272		9.93	68.5	0.244			
	1111.00					3	153	4200	0	51582		9.73	67.1	0.267			
	1111.00					4	153	6200	0		60892	9.70	66.9	0.281			
24BA032	1222.10	1.8061	1.0011	1.80	2.61	1	153	1200	0	32036		11.29	77.9	0.254	25994	0.90	5792
	1222.10					2	153	2200	0	37071		11.44	78.9	0.254			
	1222.10					3	153	4200	0	47141		12.27	84.6	0.255			
	1222.10					4	153	6200	0		57211	12.02	82.8	0.256			
24BA062	1361.30	2.0644	0.9786	2.11	2.76	1	167	1200	0	34484		9.84	67.8	0.289	28320	0.91	6248
	1361.30					2	167	2200	0	39621		10.38	71.6	0.307			
	1361.30					3	167	4200	0	49895		10.77	74.3	0.329			
	1361.30					4	167	6200	0		60169	10.64	73.3	0.338			
24BA030	1716.00	2.3213	1.4777	1.57	2.75	1	203	1200	0	27347		7.45	51.4	0.147	21481	0.88	4858
	1716.00					2	203	2200	0	32236		8.42	58.0	0.186			
	1716.00					3	203	4200	0	42012		9.07	62.5	0.206			
	1716.00					4	203	6200	0		51789	10.46	72.1	0.267			
24BA005	1727.20	1.8983	0.9944	1.91	2.75	1	203	1200	0	29555		10.48	72.3	0.225	24878	0.73	6301
	1727.20					2	203	2200	0	33452		11.37	78.4	0.258			
	1727.20					3	203	4200	0	41247		10.63	73.3	0.273			
	1727.20					4	203	6200	0		49041	10.83	74.7	0.280			
24BA034 <sup>(2)</sup>	1762.51	1.3269	0.9976	1.33	2.69	1	207	1200	0		7784	2.97	20.5	0.249	#N/A	#N/A	#N/A
	#N/A					2	#N/A	#N/A	#N/A	#N/A	#N/A	#N/A	#N/A	#N/A	#N/A	#N/A	#N/A
	#N/A					3	#N/A	#N/A	#N/A	#N/A	#N/A	#N/A	#N/A	#N/A	#N/A	#N/A	#N/A
	#N/A					4	#N/A	#N/A	#N/A	#N/A	#N/A	#N/A	#N/A	#N/A	#N/A	#N/A	#N/A
24BA037	1762.64	1.9453	0.9991	1.95	2.75	1	207	1201	0	24546		10.18	70.2	0.239	19185	0.82	4538
	1762.64					2	207	2201	0	29018		10.71	73.8	0.285			
	1762.64					3	207	4201	0	37954		10.96	75.5	0.286			
	1762.64					4	207	6200	0		46884	11.19	77.2	0.329			
24BA067 <sup>(3)</sup>	1851.67	1.7263	0.9783	1.76	2.69	1	217	1200	0	23496		9.20	63.4	0.195	18631	0.98	3922
	1851.67					2	217	2200	0	31709		9.58	66.0	0.232			
	1851.67					3	217	4200	0		42327	10.14	69.9	0.236			
	1851.67					4	217	6200	0		40303	8.04	55.5	0.217			
24BA040	1886.45	2.7251	1.4749	1.85	2.64	1	219	1200	0	18390		6.37	43.9	0.181	13526	0.76	3359
	1886.45					2	219	2200	0	22444		6.95	47.9	0.217			
	1886.45					3	219	4200	0	30551		7.33	50.6	0.251			
	1886.45					4	219	6200	0		38658	7.48	51.6	0.263			
24BA018	2063.13	2.0476	1.0019	2.04	2.77	1	237	1201	0		11603	6.99	48.2	0.202	4224	1.02	833
	2063.13					2	237	2200	0		17839	9.41	64.9	0.229			
	2063.13					3	237	4200	0		27343	11.03	76.1	0.238			
	2063.13					4	237	6200	0		41945	7.38	50.9	0.338			
18	2101.17	1.7552	0.9827	1.79	2.83	1	240	1200	0	27416		8.86	61.1	0.232	19549	1.08	3818
	2101.17					2	240	2200	0	33971		9.49	65.4	0.183			
	2101.17					3	240	4200	0	47081		10.91	75.2	0.203			
	2101.17					4	240	6200	0		60191	10.83	74.7	0.263			
24BA073	2103.62	2.0193	0.9789	2.06	2.61	1	241	1199	0	73934		13.77	94.9	0.260	63618	1.30	10845
	2103.62					2	241	2200	0	82546		12.96	89.3	0.295			
	2103.62					3	241	4200	0	99753		12.93	89.2	0.290			
	2103.62					4	241	6200	0		116960	12.86	88.7	0.311			

Table 1: Results of multi-Stage testing. Continued in table 2.

Sample Number	Depth [m]	Sample Length [in]	Sample Diameter [in]	L:D Ratio	As-Tested Bulk Density [g/cm <sup>3</sup> ]	Stage	Set Point Temperature [°F]	Confining Pressure [psi]	Pore Pressure [psi]	Scaled Compressive Strength [psi]	Compressive Strength [psi]	Static Young's Modulus [Mpsi]	Static Young's Modulus [GPa]	Poisson's Ratio <sup>(1)</sup>	Estimated UCS [psi]	Coefficient of Friction [-]	Cohesive Strength [psi]
8	2242.41	1.8884	0.9804	1.93	2.71	1	254	1200	0	19556		6.13	42.2	0.245	16094	0.55	4738
	2242.41					2	254	2200	0	22440		6.54	45.1	0.262			
	2242.41					3	254	4200	0	28209		6.85	47.3	0.246			
	2242.41					4	254	6200	0		33978	7.65	52.8	0.289			
Hunt Well #13	2352.26	2.3583	1.5002	1.57	2.60	1	265	1200	0	48981		5.86	40.4	0.282	40140	1.17	7394
	2352.26					2	265	2200	0	56349		7.15	49.3	0.304			
	2352.26					3	265	4200	0	71084		8.76	60.4	0.328			
	2352.26					4	265	6200	0		85820	9.33	64.4	0.332			
Hunt Well #18	2355.62	2.3269	1.5014	1.55	2.68	1	266	1200	0	37989		4.37	30.1	0.284	29241	1.16	5415
	2355.62					2	266	2200	0	45279		6.23	43.0	0.334			
	2355.62					3	266	4200	0	59859		8.07	55.6	0.336			
	2355.62					4	266	6200	0		74439	9.52	65.7	0.330			
Hunt Well #21	2357.38	2.3169	1.5008	1.54	2.71	1	266	1200	0	38924		7.58	52.3	0.288	28767	1.28	4944
	2357.38					2	266	2200	0	47388		9.99	66.9	0.325			
	2357.38					3	266	4200	0	64316		10.71	73.8	0.330			
	2357.38					4	266	6200	0		81245	11.14	76.8	0.349			
Hunt #27	2361.00	2.2715	1.5011	1.51	2.64	1	266	1200	0	41490		4.84	33.4	0.270	33497	1.10	6490
	2361.00					2	266	2200	0	48150		6.89	47.5	0.333			
	2361.00					3	266	4200	0	61471		8.40	57.9	0.332			
	2361.00					4	266	6200	0		74793	9.47	65.3	0.337			
24BA004	2556.30	3.0168	1.4743	2.05	2.70	1	286	1200	0	41747		11.37	78.4	0.190	33061	1.16	6144
	2556.30					2	286	2200	0	48985		11.92	82.2	0.230			
	2556.30					3	286	4200	0	63461		11.86	81.7	0.247			
	2556.30					4	286	6200	0		77938	11.49	79.2	0.251			
24BA069	2786.65	1.9881	0.9787	2.03	2.66	1	308	1200	0	38058		10.47	72.2	0.259	32113	0.89	7214
	2786.65					2	308	2200	0	43012		11.85	81.7	0.266			
	2786.65					3	308	4200	0	52920		11.86	81.8	0.254			
	2786.65					4	308	6200	0		62828	12.21	84.2	0.288			
BCS 1	3025.50	2.1688	1.4958	1.45	2.46	1	332	1201	0		11349	3.73	25.7	0.276	3218	1.12	608
	3025.50					2	332	2201	0		18911	5.51	38.0	0.266			
	3025.50					3	332	4200	0		31544	6.66	45.9	0.254			
	3025.50					4	332	6197	0		46257	4.48	30.9				
BCS2_S1	3025.70	2.2134	1.4976	1.48	2.46	1	332	1200	0	25941		6.24	43.0	0.131	17425	1.14	3270
	3025.70					2	332	2200	0	33039		7.62	52.6	0.181			
	3025.70					3	332	4200	0	47233		7.41	51.1	0.174			
	3025.70					4	332	6200	0		61428	8.22	56.7	0.180			
16	3027.20	1.6168	0.9823	1.65	2.48	1	332	1200	0	19535		4.52	31.2	0.187	15511	0.64	4235
	3027.20					2	332	2201	0	22892		5.08	35.0	0.256			
	3027.20					3	332	4200	0	29597		5.61	38.7	0.240			
	3027.20					4	332	6200	0		36305	5.70	39.3	0.274			
24BA002_S1	3526.10	2.8473	1.4758	1.93	2.76	1	382	1200	0	29929		8.27	57.0	0.207	21975	1.09	4268
	3526.10					2	382	2200	0	36557		9.43	65.0	0.222			
	3526.10					3	382	4200	0	49814		9.82	67.7	0.275			
	3526.10					4	382	6200	0		63071	10.38	71.5	0.260			
9	3603.01	1.6933	0.9811	1.73	2.75	1	389	1200	0	19728		9.77	66.9	0.176	15724	0.64	4304
	3603.01					2	389	2200	0	23065		10.88	75.0	0.170			
	3603.01					3	389	4200	0	29740		9.27	63.9	0.175			
	3603.01					4	389	6200	0		36414	11.52	79.4	0.187			

Table 2: Results of multi-stage testing. Continued from table 1.

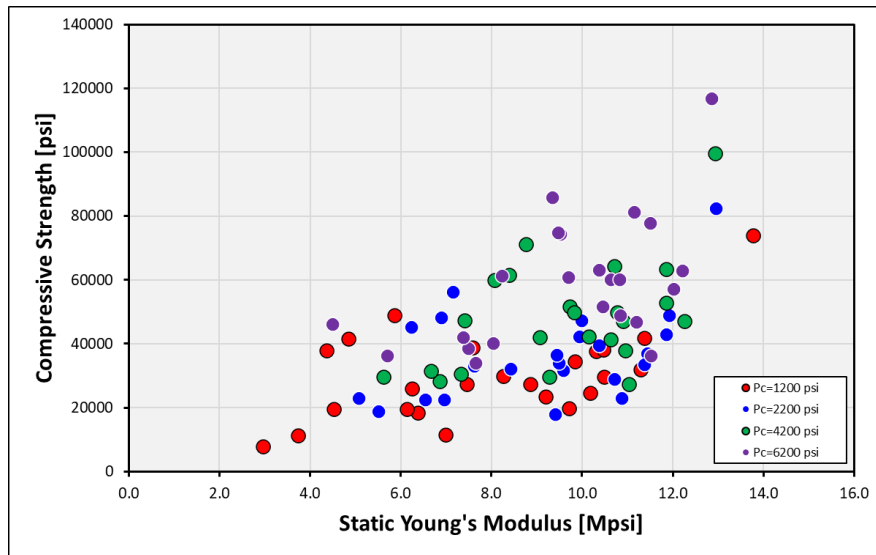


Figure 10: The correlation between increasing static Young's modulus and compressive strength is well observed in the specimens tested as part of this project.

Sample Number [-]	Depth [m]	Sample Length [in]	Sample Diameter [in]	L:D Ratio [-]	As-Tested Bulk Density (g/cm <sup>3</sup> )	Initial Temperature [°C]	Final Temperature [°C]	Confining Pressure [psi]	Pore Pressure [psi]	Axial Thermal Expansivity <sup>(2)</sup> [in/in/°C]
24BA082	1526.64	2.0210	0.9778	2.07	2.67	30.0	84.0	1725	0	-7.87E-06
24BA028	1789.40	1.9770	0.9910	1.99	2.56	30.0	99.0	2032	0	-5.02E-06
24BA064	1826.14	2.0140	0.9800	2.06	2.61	30.0	101.1	2082	0	-6.39E-06
24BA026	1846.80	2.0260	1.0030	2.02	2.93	30.0	102.0	2097	0	-6.88E-06
5	1833.33	2.0040	0.9830	2.04	2.59	29.7	101.0	2073	0	-4.58E-06
13	1893.28	1.9920	0.9840	2.02	2.60	30.0	104.1	2152	0	-5.88E-06
15	1896.10	2.0140	0.9830	2.05	2.68	30.0	105.1	2152	0	-5.97E-06
19	2101.09	2.0130	0.9860	2.04	2.66	30.0	116.0	2393	0	-6.17E-06
18b	2101.17	1.9440	0.9840	1.98	2.74	30.0	116.0	2152	0	-7.31E-06
16b	3027.20	1.9680	0.9820	2.00	2.46	30.0	167.0	3443	0	-7.15E-06

Table 3: Results of thermal expansivity testing, conducted by Metarock Laboratories, Houston TX.

Sample Number	Depth	Confining Pressure	Sample Temperature	Bulk Density	Acoustic Velocity <sup>(1)</sup>				Dynamic Bulk Modulus	Dynamic Young's Modulus	Dynamic Shear Modulus	Dynamic Poisson's Ratio	Vp/Vs
					Compressional		Shear						
[-]	[m]	[psi]	[°C]	[g/cm³]	[ft/sec]	[us/ft]	[ft/sec]	[us/ft]	[Mpsi]	[Mpsi]	[Mpsi]	[-]	[-]
24BA082	1526.64	1725	30.0	2.67	19566	51.1	11723	85.3	7.17	12.05	4.94	0.22	1.67
	1526.64	1725	84.0	2.67	19326	51.7	11627	86.0	6.94	11.82	4.86	0.22	1.66
24BA028	1789.40	2032	30.0	2.56	16026	62.4	11485	87.1	2.79	8.84	4.55	-0.03	1.40
	1789.40	2032	99.0	2.56	15477	64.6	11111	90.0	2.58	8.24	4.25	-0.03	1.39
24BA064	1826.14	2082	30.0	2.61	18358	54.5	12133	82.4	4.95	11.51	5.17	0.11	1.51
	1826.14	2082	101.1	2.61	18130	55.2	11999	83.3	4.81	11.24	5.06	0.11	1.51
24BA026	1846.80	2097	30.0	2.93	22323	44.8	12353	81.0	11.65	15.43	6.03	0.28	1.81
	1846.80	2097	102.0	2.93	21955	45.5	12132	82.4	11.29	14.89	5.82	0.28	1.81
5	1833.33	2073	30.0	2.59	19917	50.2	11047	90.5	8.15	10.87	4.25	0.28	1.80
	1833.33	2073	101.0	2.59	19910	50.2	11043	90.6	8.15	10.86	4.25	0.28	1.80
13	1893.28	2152	30.0	2.60	19970	50.1	13289	75.2	5.72	13.65	6.19	0.10	1.50
	1893.28	2152	104.1	2.60	19742	50.7	13146	76.1	5.58	13.34	6.06	0.10	1.50
15	1896.10	2152	30.0	2.68	20046	49.9	12123	82.5	7.44	12.87	5.31	0.21	1.65
	1896.10	2152	105.0	2.68	19682	50.8	11878	84.2	7.20	12.38	5.10	0.21	1.66
19	2101.09	2393	30.0	2.66	19409	51.5	11682	85.6	6.99	11.91	4.90	0.22	1.66
	2101.09	2393	116.0	2.66	18983	52.7	11451	87.3	6.66	11.42	4.70	0.21	1.66
18b	2101.17	2152	30.0	2.74	20819	48.0	12402	80.6	8.44	13.93	5.69	0.22	1.68
	2101.17	2152	116.0	2.74	20413	49.0	12114	82.5	8.17	13.33	5.43	0.23	1.69
16b	3027.20	3443	30.0	2.46	16046	62.3	10328	96.8	3.83	8.12	3.54	0.15	1.55
	3027.20	3443	167.0	2.46	15358	65.1	9758	102.5	3.62	7.35	3.16	0.16	1.57

Table 4: Results of ultrasonic velocity measurement conducted in conjunction with thermal expansivity.

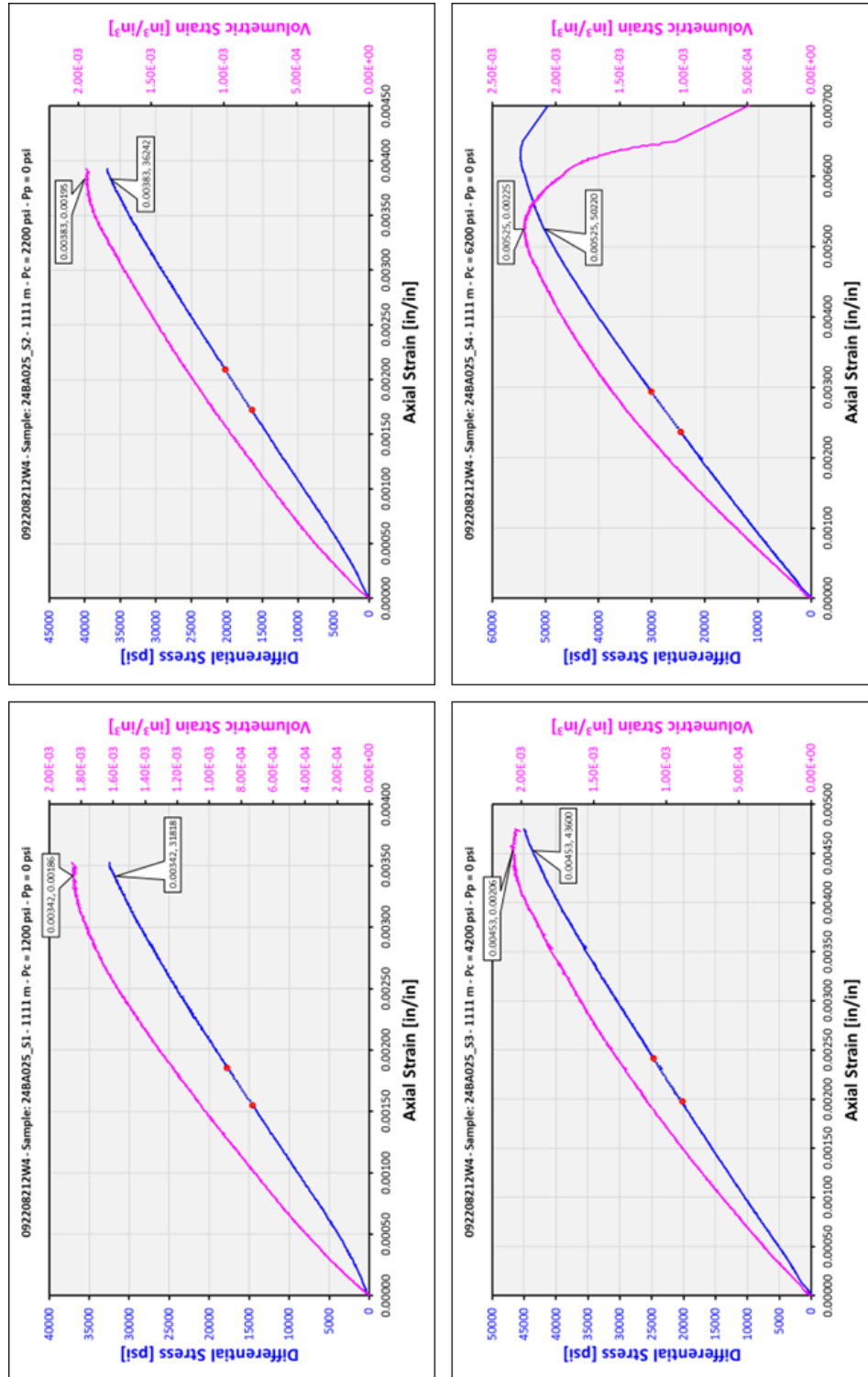


Figure 11: Results of the four separate stages of a multi-stage test performed using the volumetric strain procedure on specimen 24BA025 (Depth 1111.00 m). During each confining pressure stage (1200, 2200, 4200, and 6200 psi) the specimen was loaded axially until we observed the transition from volumetric compression to dilation, at which point axial load was removed and a higher confining pressure is applied. Axial loading during Stage 4 is continued until shear failure is observed.

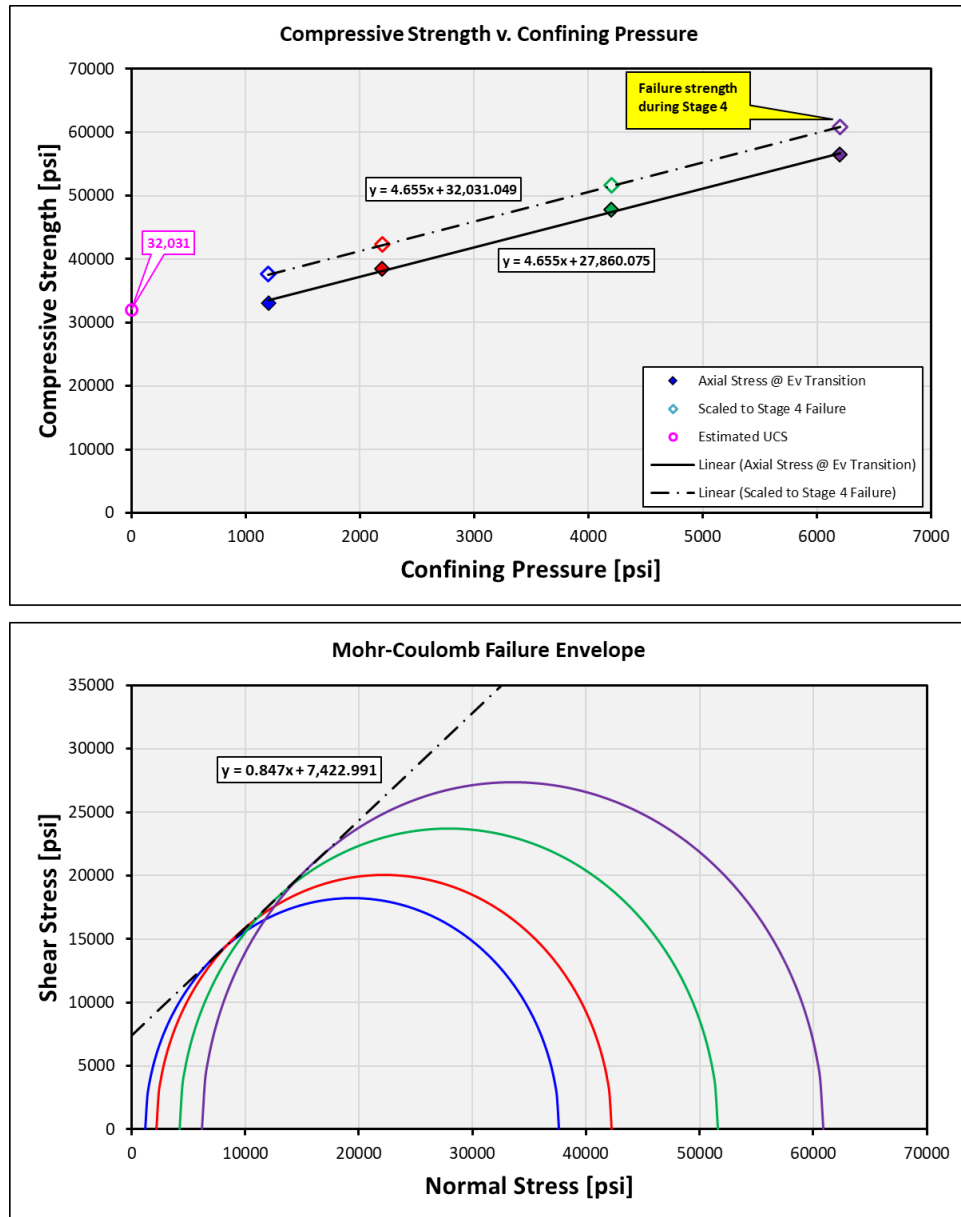


Figure 12: Top - Results of multi-stage testing on specimen 24BA025, showing the axial stress at the ev transition, and those results scaled to the Stage 4 failure strength. Bottom - Mohr-Coulomb failure envelope generated using the results shown in the Top plot, indicating a coefficient of friction of ~0.85 and a cohesive strength of ~7433 psi.

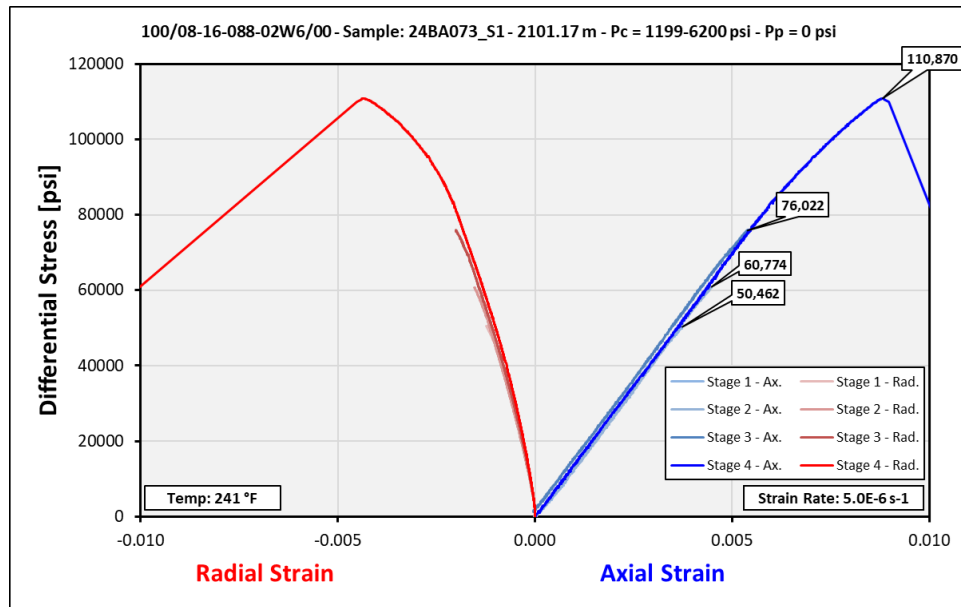


Figure 13: Stress-Strain curves for the multi-stage test on specimen 24BA073, the strongest tested as part of this project. Test was conducted at ~241 °F using a nominal strain rate of  $5 \times 10^{-6}$ /s.

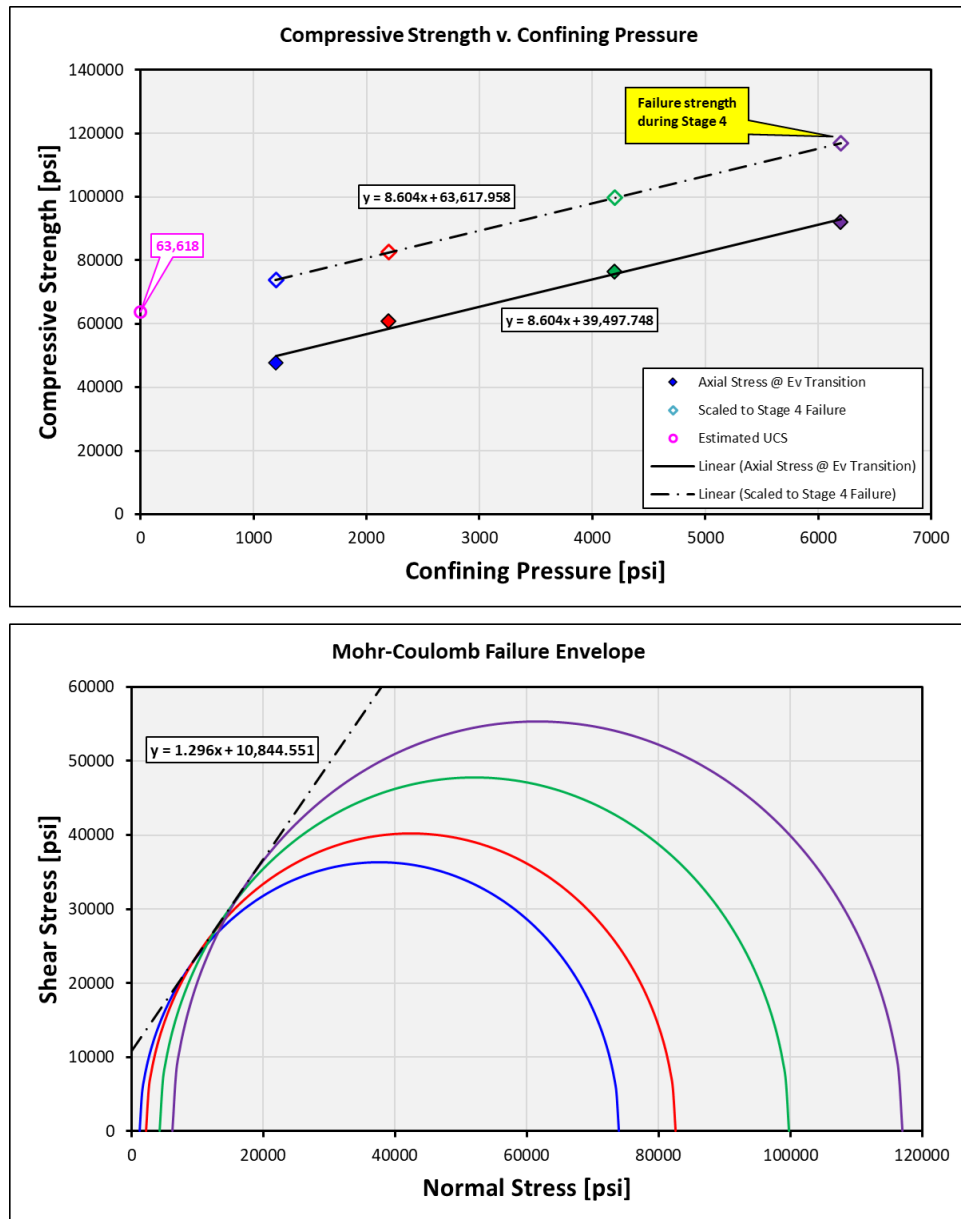


Figure 14: Top - compressive strength v. failure for specimen 24BA073, the strongest specimen tested. Trend of Strength v.  $P_C$  is not unusual, nor is the degree of scaling from the axial stress at  $e_v$  transition up to failure strength. Bottom - Mohr-Coulomb envelope for 24BA073. The fit of this envelope is good, though the coefficient of friction of the intact rock is remarkably high.